# Kinetics of the Formation of Silver Dimers: Early Stages in the Formation of Silver Nanoparticles

Kevin G. Stamplecoskie and Juan C. Scaiano*

Centre for Catalysis Research and Innovation, Department of Chemistry, University of Ottawa, Ottawa, Ontario K1N 6N5, Canada

Ⓢ *Supporting Information*

ABSTRACT: Silver clusters too small to support a plasmon band possess interesting fluorescence properties as well as being a convenient route to studying the early stages of nanoparticle formation. Fluorescent silver clusters are synthesized in toluene solution, and the formation is monitored herein by laser flash photolysis (LFP). Kinetic analysis of the formation of the Ag clusters is consistent with the formation of the smallest possible clusters, silver dimers (Ag_2), whereby a mechanism for the formation of these clusters is provided as well as the first reported extinction coefficient and association constant for Ag^0 to form Ag_2. The formation of Ag_2 clusters is contrasted with the formation of Ag nanoparticles in aqueous media, and the particular stability and selectivity toward Ag_2 in this system is also studied using LFP.
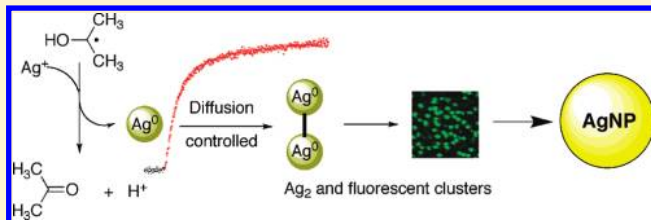
INTRODUCTION

Small agglomerates of metal atoms containing from 2 to ∼100 atoms are often referred to as clusters, and they provide an important link between metal atoms and nanoparticles.[1] Small metal clusters, on the order of the de Broglie wavelength of the Fermi level (which is ∼0.5 nm for Ag and Au), are known to exhibit strong fluorescence that can be tuned across the visible spectrum by controlling the size of the metal clusters.[1,2] Fluorescent metal clusters (e.g., Ag_x) may provide a less toxic alternative to semiconductor quantum dots as bright emissive labels in biology and medicine, as well as being used in chemical sensing and single-molecule studies.[3,4] We recently synthesized solutions containing silver nanoparticles (AgNP) that exhibit strong absorption centered at 450 nm and can be excited to produce intense emission centered at 540 nm.[5] The lifetime of AgNP plasmons is very short, on the femtosecond time scale,[6] whereas the 540 nm emission in the AgNP solution described here was determined to have more molecular-type properties, fitting a monoexponential function with a lifetime of 2.6 ± 0.1 ns. Therefore, the emission at 540 nm has been attributed to silver dimer (Ag_2) clusters in the AgNP solution and not the AgNP themselves. In fact, other reports have detected Ag cluster emission,[1−3,7] which is known to be enhanced when the clusters are bound to AgNP.[8]

As mentioned above, metal clusters are an important bridge between atomic metals and nanoparticles, and as such clusters provide a route to understanding the mechanism of nucleation and growth of metal nanoparticles. Also, in order to use fluorescent Ag_x clusters in many applications like imaging and biology, it is of particular interest to understand the mechanism of formation of Ag_2 clusters and the particular stability of these clusters in fluorescent silver nanoparticle (AgFNP) solution. The kinetics of the formation of the 450 nm absorption signal, attributed to Ag_2 clusters, was studied using laser flash photolysis (LFP) techniques. Briefly, the photochemical reaction for the formation of Ag clusters is initiated with a laser pulse, and the transient absorbance change (ΔOD) at 450 nm is monitored on short time scales (microseconds) after the laser pulse. The kinetic analysis of the transient signal is consistent with the formation of Ag_2 clusters as the fluorescent species, and a possible mechanism of formation is provided. The first reported formation constant for Ag dimers as well as an extinction coefficient for Ag_2 is also reported here.

RESULTS

Scheme 1 depicts the expected reactions that occur in a typical LFP experiment when I-2959, a commercial photochemical reducing agent, is excited by a 355 nm laser pulse, eventually leading to the formation of Ag_2 clusters.

Transient spectra for the change in absorbance of LFP solutions (see Experimental Section) after a 355 nm, 6 ns laser pulse are shown in Figure 1. Also shown in Figure 1 is an absorption spectrum for the AgFNP solution taken after it was completely photolyzed with UVA irradiation in a Luzchem photoreactor, and the spectrum shows an absorption maximum at 450 nm similar to that obtained in the LFP experiments at short time scales. Larger Ag clusters show longer wavelength absorption maxima as the cluster size increases.[2] Therefore, the fact that the 450 nm absorption maximum never shifts suggests that the immediately formed Ag_2 clusters not only are stable but also are the major absorbing chromophore in solution. The change in absorbance at 450 nm in an LFP experiment is plotted in Figure 1 (inset); kinetic analysis gives a good fit to a
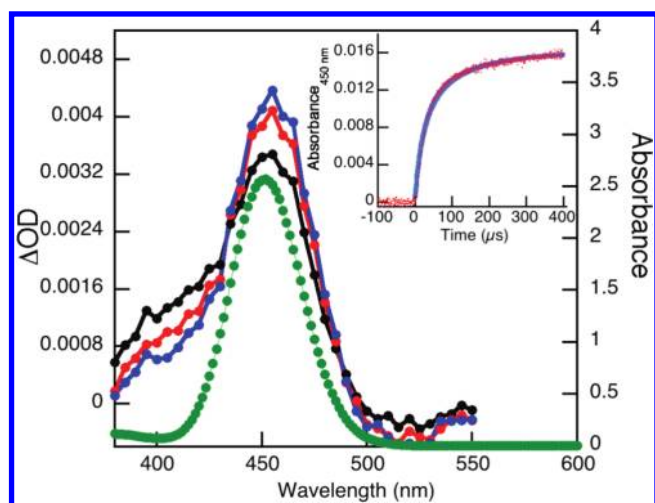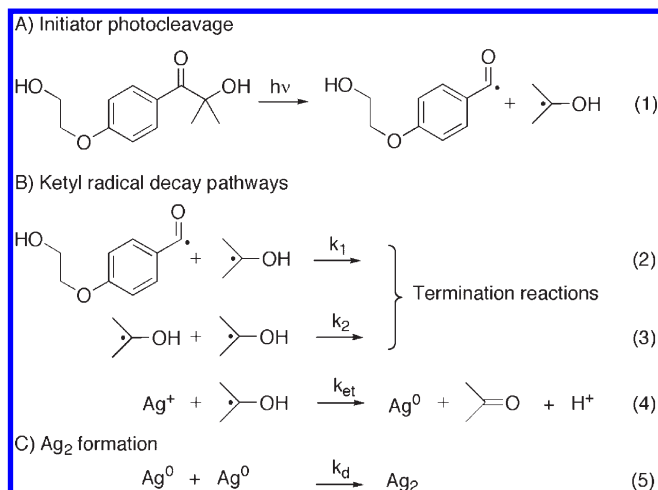
Figure 1. LFP experimental data: transient spectra (left axis) recorded 200 (black), 500 (red), and 750 μs (blue) after the 355 nm laser pulse, overlaid with the spectrum (right axis) from a stable AgFNP solution in toluene long after irradiation. Also shown in the inset is the change in absorbance at 450 nm of an LFP solution after a 355 nm laser pulse (red) fit to a second-order rate law (blue).

Scheme 1. Key Reactions Leading to Ag$_2$ Formation

Figure 2. Growth in 450 nm absorbance with different 355 nm laser doses and (inset) plot of the plateau ΔOD (determined from the kinetic fit) versus the square root of the laser dose for a typical LFP solution in toluene.

second-order rate law (correlation factor = 0.995) with a value of $2k_d/\varepsilon_{Ag_2} = 1.9 \times 10^6$ cm s^{-1}. The second-order behavior for the formation of the optical signal at 450 nm is consistent with two reduced silver atoms associating as shown in Scheme 1. However, in order to obtain an absolute rate constant, it is necessary to determine the extinction coefficient for Ag$_2$. It is also interesting to note that, if one turns off the monitoring beam in LFP and records the emission intensity after exciting the species that forms and absorbs at 450 nm (experimental details and data in the Supporting Information), the intensity of the fluorescent emission from the Ag$_2$ clusters also increases at the same rate and overlaps with the increase in absorption at 450 nm (Figure S2a in the Supporting Information).

To better understand the kinetics of Ag$_2$ formation, the intensity of the excitation laser was varied, which is equivalent to changing the initial ketyl radical concentration (reaction 1 in Scheme 1). The maximum 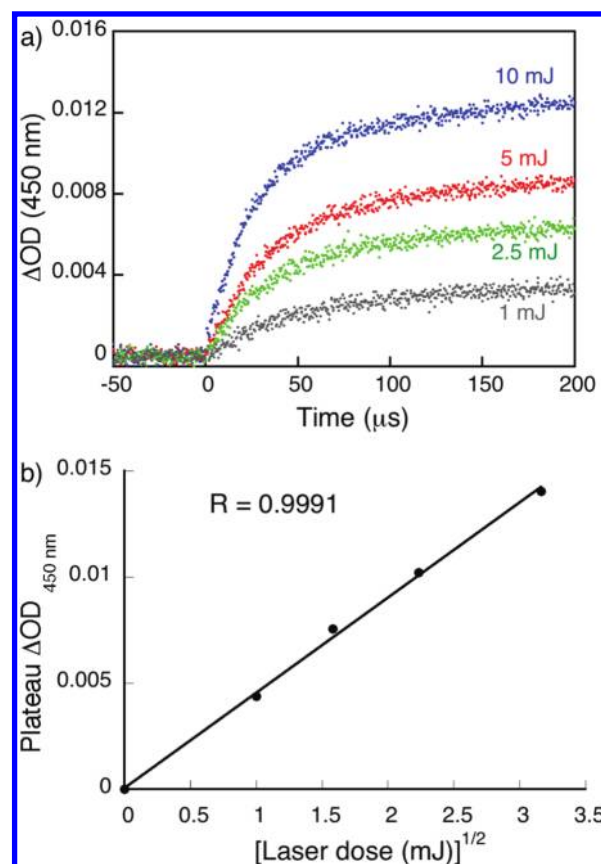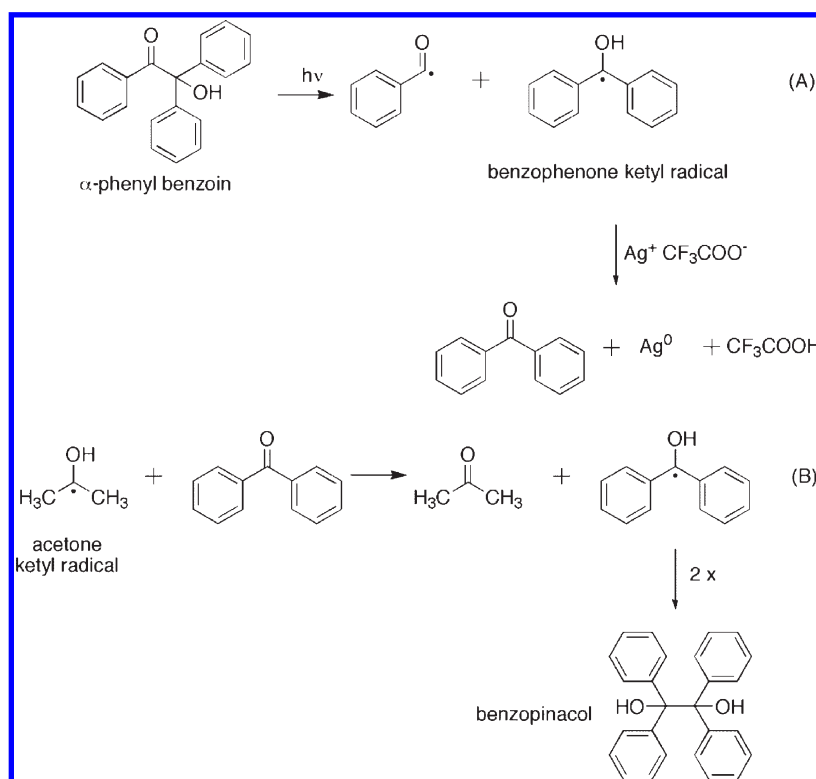absorbance at long times after a laser pulse, and thus the final concentration of Ag$_2$, followed a square root law with the laser dose, as shown in Figure 2. The square root dependence was initially intriguing, as one could expect the total formation of Ag$_2$ to depend linearly on the laser power (i.e., the initial ketyl radical concentration). However, the square root dependence is a common result for photochemically generated radicals with competing terminating and product-forming reactions where the terminating reactions are fast (reactions 2 and 3 in Scheme 1 are known to be diffusion-controlled).[9]

The above result suggests that the rate constant for the electron transfer from the ketyl radical to Ag$^+$ (reaction 4 in scheme 1) is slower than the diffusion-controlled termination reactions (reactions 2 and 3 in Scheme 1) but does not give an estimate of the actual value of the rate constant. The ketyl radical generated from photolysis of α-phenylbenzoin (Scheme 2) is a weaker reducing agent than the isopropyl radical used here. This is known from the fact that radiolysis of isopropanol solutions of benzophenone give benzopinacol as the only product, as shown in Scheme 2B.[10] However, the advantage here is that the ketyl radical generated from photolysis of α-phenylbenzoin is easily observable in LFP, with an absorption maximum at 545 nm. Scheme 2A depicts how α-phenylbenzoin is used to generate a reducing radical and shows the proposed subsequent quenching by AgCF$_3$COO.

A nitrogen-purged 5 mM solution of α-phenylbenzoin in toluene was excited by a 355 nm laser, and the transient spectrum in Figure 3a and the change in ΔOD at 545 nm due to the

3914

dx.doi.org/10.1021/ja108451v |*J. Am. Chem. Soc.* 2011, 133, 3913–3920

Scheme 2. Quenching of the Benzophenone Ketyl Radical Derived from α-Phenylbenzoin by Ag$^+$

benzophenone ketyl radical transient decay, as shown in Figure 3b, were recorded. The transient absorption spectrum has an absorption maximum at ∼540 nm that corresponds well with that of the benzophenone ketyl radical.[11] Also shown in Figure 3b is the transient decay in the presence of 0−500 mM AgCF$_3$COO, which shows no significant quenching of the ketyl radicals. This implies that the transfer of an electron from an α-hydroxyl radical to Ag$^+$ in toluene is much slower than diffusion control.

Until this point, what has been shown is that reaction 1 in Scheme 1 is considered instantaneous (during the laser pulse) and reactions 2 and 3 are known to be diffusion controlled, while reaction 4 is comparatively very slow ($k_{et} \ll k_1 + k_2$). Also, we observe clean second-order kinetics for the formation of Ag$_2$, but without an extinction coefficient for Ag$_2$ the rate constant for Ag^0 dimerization (k_d) cannot be determined. In order to obtain ε_{Ag_2}, bromothymol blue (BTB-H) was used as an indicator to measure the amount of the base form of CHA remaining in AgFNP solutions. Scheme 3 shows how CHA acts as a proton sink when Ag$^+$ is reduced by the ketyl radical. Also shown in Scheme 3 (reaction 7) is how BTB-H can be used as an indicator of the amount of CHA in the base form, and thus to quantify the amount of reduced Ag in solution.

Using BTB-H as an indicator of CHA, the change in absorption spectrum recorded after the addition of aliquots of an AgFNP solution (that was never photolyzed and so had no reduced AgCF$_3$COO)) is shown in Figure 4a. Further details are given in the Experimental Section. The change in absorption indicates the amount of CHA in the basic form in solution (since CHA has a pK_a of 10.6 and bromothymol blue has a pK_a of 7.0)[12] by deprotonating the BTB-H (to BTB) indicator and causing the observed color change. However, after reaction 6 in Scheme 3,

CHA is protonated and is no longer available to deprotonate BTB-H. Overall, by comparing an LFP solution that has been photolyzed with one that has not, the change in CHA can be correlated with a concentration of H$^+$ produced as in Scheme 3. Since H$^+$ and Ag^0 are produced in equimolar quantities, the measure of H$^+$ is also a measure of Ag^0 produced. Repeating this experiment several times and plotting the absorbance at 450 nm of the AgFNP solutions (Figure 4b) versus the determined concentration of Ag$_2$ (from Figure 4a), the extinction coefficient for Ag$_2$ is then taken as the slope of the linear best fit, as shown in Figure 4b (inset), which is $\varepsilon_{Ag_2} = 25\,400 \pm 2600$ M^{-1}cm^{-1}.

With the extinction coefficient it was determined that the rate constant for the formation of Ag$_2$ is then $k_d \approx (2.4 \pm 0.24) \times 10^{10}$ M^{-1} s^{-1}. Using the Debye equation, diffusion-controlled reactions in toluene are found to have a rate constant of 1.1×10^{10} M^{-1} s^{-1}, and so the rate constant determined here can be approximated as a diffusion-controlled association of Ag^0 into dimers.[13]

In further exploration of the stability/reactivity of the Ag$_2$ clusters at short time scales, two types of experiments were performed: no-flow experiments and two-laser experiments.

In the no-flow experiments, a typical LFP experiment was performed, with the only modification being that the solution was static rather than flowing through the cuvette, thus forcing the accumulation of Ag$_2$. The sample was exposed to 10 laser shots, and the data were averaged. The recorded data are shown in Figure 5, leading to observable bleaching of the sample, following by recovery; the bleaching signals are largely acquired in the later shots, as Ag$_2$ accumulates. Bleaching refers to the reduction in sample absorbance upon laser excitation and is common in LFP. In this case, the transient ΔOD at 450 nm was monitored (Figure 5), revealing bleaching of the 450 nm signal

followed by recovery and growth of the signal that again followed a second-order growth with the same rate as for the flow solutions.

In the two-laser experiments, two separate 355 nm laser pulses, separated in time by 200 μs, were used to photolyze a flowing LFP solution, with the resultant change in ΔOD at 450 nm shown in Figure 6a; note that no significant flow takes place in 200 μs, so that for practical purposes the solution is static in this time scale. In this experiment, the Ag_2 generated from the first laser pulse will be present during the second laser pulse, which generates additional ketyl radicals and thus Ag^0. We observed that the growth in ΔOD after each laser pulse (fresh solution or after one laser pulse) occurs at the same rate, with
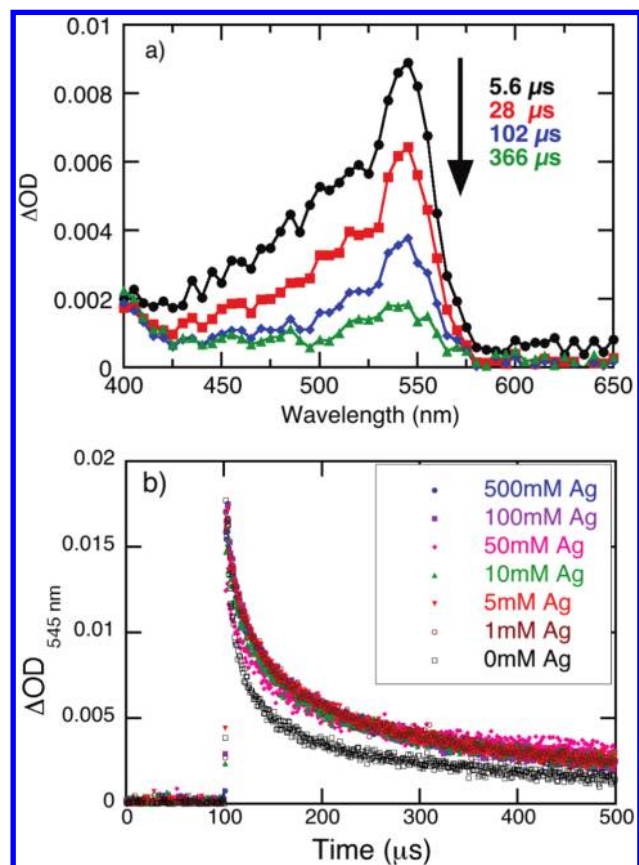

Figure 3. (a) Transient absorption spectrum for the benzophenone α-hydroxyl radical at 5.6 (black), 28 (red), 102 (blue), and 366 μs (green) after the laser pulse, and (b) corresponding decay traces of the 545 nm absorption upon quenching with various concentrations of $AgCF_3COO$.
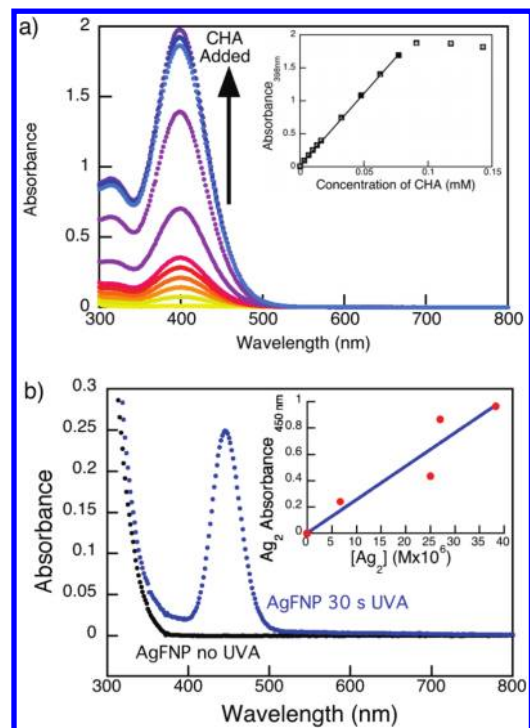

Figure 4. (a) Absorbance spectra of BTB-H/BTB upon addition of AgFNP solution, starting with no AgFNP added (yellow) and ending when the BTB-H/BTB is completely deprotonated by CHA (blue), as well as (inset) a plot of the change in absorbance at 400 nm due to BTB plotted versus the concentration of CHA added from an AgFNP solution that was never irradiated (gray) and from one that was irradiated for 30 s with UVA (black). (b) Absorbance of the AgFNP solution before (black) and after irradiation (blue) with UVA. Inset: absorbance for AgFNP solutions plotted against calculated Ag_2 concentrations.

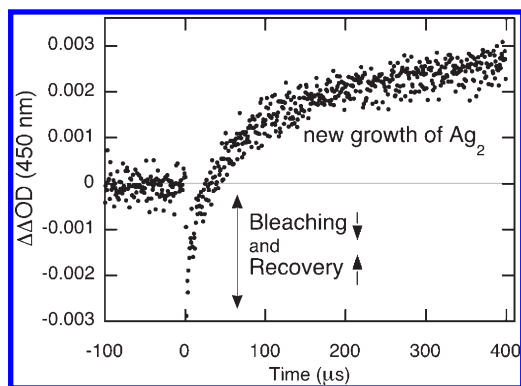**Scheme 3. Photochemical Formation of Ag_2: CHA as a Base**
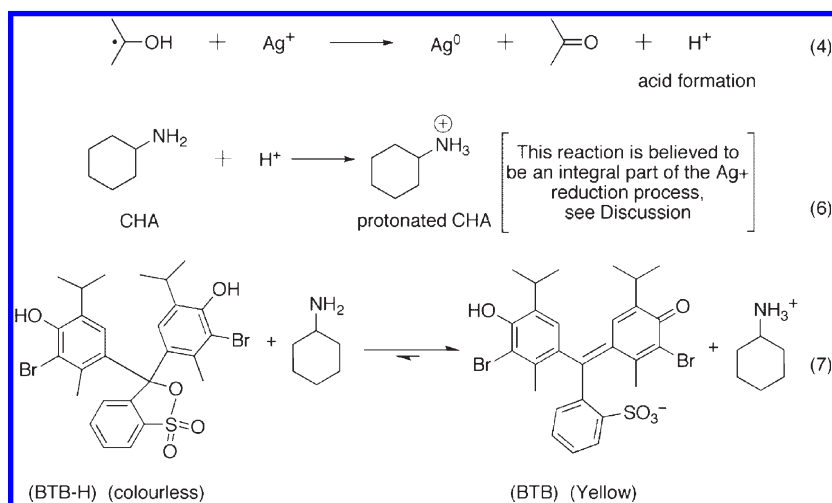
Figure 5. Transient absorption of 450 nm light for an AgFNP solution without flow, showing the bleach and recovery of the 450 nm signal and formation of more Ag_2. The solution contained 5 mM I-2959 and CHA, and 10 mM $AgCF_3COO$ in toluene. The laser was pulsed at 1 Hz, and the signal was obtained as an average of 10 consecutive pulses without flowing fresh solution between pulses. Bleaching signals may be slightly enhanced by emission from accumulated photoproducts.
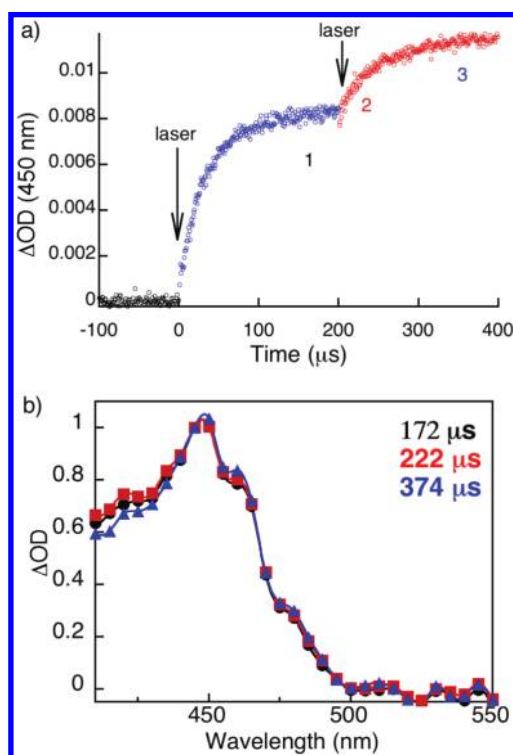

Figure 6. (a) Transient absorption for a flowing AgFNP solution in toluene irradiated with two 355 nm laser pulses separated in time by 200 μs, and (b) transient absorption spectrum of the same two-laser LFP experiment at the times labeled in (a). A slight bleaching occurs with the second laser (beginning of red trace).

both growth curves fitting a second-order rate law. The differences observed in total ΔOD are the result of a lower intensity second laser pulse, which generates fewer ketyl radicals, and thus less Ag_2. The normalized absorbance spectrum at the times indicated by the numbers 1 (172 μs), 2 (222 μs), and 3 (374 μs) in Figure 6a are plotted in Figure 6b, showing that there is also no difference in absorbance spectra between laser pulses as well.

In order to rule out the possibility that the signal at 450 nm in AgFNP solutions is from a plasmon absorption, silver

nanoparticles were formed in a typical LFP setup using a 266 nm laser. In this case the growth of the plasmon absorption, and therefore the nanoparticles, is followed by an increase in absorption at 420 nm. It should be noted that flow solutions containing $AgNO_3$ and I-2959 showed no change in absorbance on the time scales monitored by LFP (up to ~5 ms after the laser pulse). This result indicates that AgNP cannot form large enough particles to support a plasmon absorption within the time scale of these experiments. However, when the solution was not flowed, the black trace shown in Figure 7c was obtained. This is likely due to the fact that nanoparticles large enough to support a plasmon absorption require slow nucleation steps that are too long to be monitored on short time scales after a single laser pulse. However, when the solution is not flowed, what is monitored is actually the addition of Ag^0 to AgNP seeds already formed in earlier laser pulses. A typical transient absorption spectrum for both fluorescent and nonfluorescent AgNP solutions is shown in Figure 7a, and a steady-state UV−vis absorption spectrum of each is given in Figure 7b for comparison. It is clear in Figure 7a,b that the absorption spectrum for the silver plasmon not only appears at shorter wavelengths but also has to be monitored at much longer times than the AgFNP signal due to the slower growth. The red shift in the absorption maximum when AgNP are formed is indicative of the formation of larger AgNP as Ag^0 adds, which is again not observed for the signal attributed to Ag_2 in the AgFNP solutions.[14] It is also interesting to note that the spectra in Figure 7b for both AgFNP and nonfluorescent AgNP, after UV irradiation, show in both cases that the transient signal corresponds well with the long-term spectrum of each. Finally, shown in Figure 7c is a comparison between the transient signals for an AgFNP solution (monitored at 450 nm) and a nonfluorescent AgNP solution (monitored at 420 nm). It is clear from the comparison of the two traces that the appearance of the plasmon occurs on a drastically different time scale and with a much lower final intensity than the formation of the 450 nm signal for Ag_2. In fact, in the case of AgFNP in toluene or THF, our earlier work showed that, on long time scales, small nanoparticles are formed (~3.4 nm), surrounded by highly fluorescent clusters.[5]

■ DISCUSSION

Small silver clusters provide a valuable link between atomic metals and nanoparticles. Thus, studying the mechanism of formation of these clusters can be a convenient way of determining the initial stages of nanoparticle formation in systems such as the one here (organic solvent with amine stabilizing agent). The first step in determining the mechanism of the formation of Ag_2 is therefore to determine the kinetic parameters given in Scheme 1. The termination reactions (2 and 3) of Scheme 1 are known to be limited by diffusion and spin statistics.[15] However, none of the compounds in reaction 4 are expected to give an absorption that can be easily monitored in toluene by LFP. Further, the extinction coefficient for Ag_2 was previously unknown, yet Ag_2 is the only species readily detectable in Scheme 1. While we were able to measure $2k_d/\varepsilon_{Ag_2}$, the determination of an absolute rate constant required a procedure to evaluate ε_{Ag_2}.

Figure 1 (inset) shows that the increase in absorption at 450 nm attributed to Ag_2 formation fits extremely well to a second-order rate law. Small silver clusters have been previously reported to have lower energy absorption maxima than the plasmon of AgNP and extinction coefficients similar to the values determined here. Specifically, Vosch and Xu have observed larger
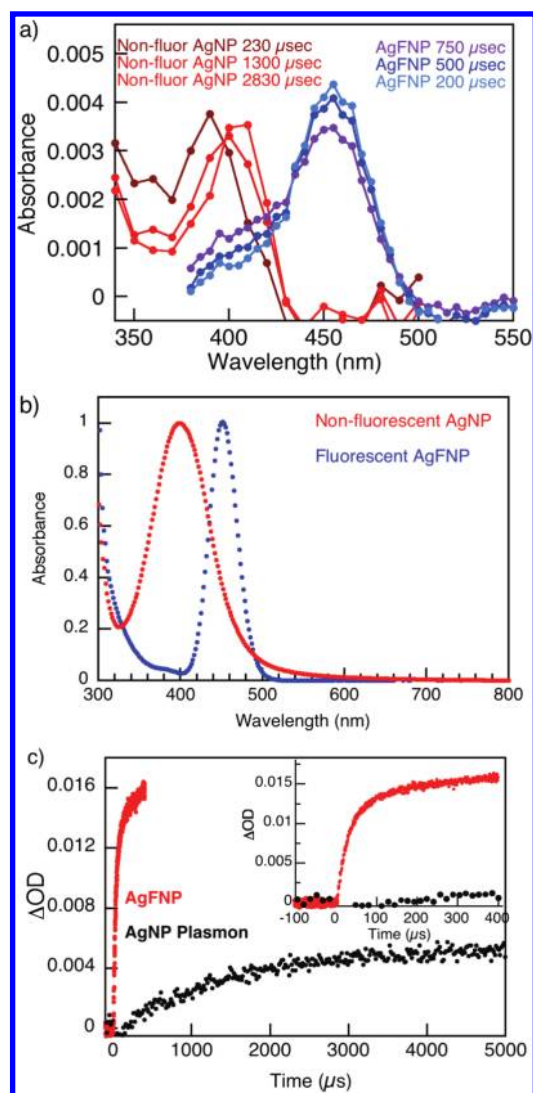
Figure 7. (a) Comparison of the transient absorption spectra recorded by LFP in the formation of nonfluorescent AgNP in water with those of AgFNP in toluene. (b) Comparison of the absorption spectra after long irradiation times of an AgFNP solution in toluene with those of ∼3.3 nm nonfluorescent citrate-stabilized AgNP in water (normalized wiht respect to each maximum). (c) Comparison of the transient absorption obtained upon photolysis, forming AgNP in water, monitored at 410 nm with that of the AgFNP solutions in toluene monitored at 450 nm.

Ag clusters, with an extinction coefficient of 32 000 M^{-1} cm^{-1}, that absorb in the visible region at energies lower than spherical AgNP plasmon absorptions.[2,16] Using the extinction coefficient for Ag$_2$, estimated from titration of a solution of BTB-H, gives a rate constant for the formation of Ag–Ag dimers of 2.4×10^{10} M^{-1} s^{-1}, which is on the order of diffusion-controlled reactions in toluene.

These experiments to determine the extinction coefficient involve four approximations:

1 That at low conversion and at 450 nm, the absorbance at 450 nm is directly proportional to the concentration of Ag$_2$ formed and the amount of Ag$^+$ reduced.
2 That the absorbance of Ag$_2$ follows Beer's law.
3 That no protons are lost to chemistry other than the protonation of CHA (see Scheme S1).

4 That any plasmonic enhancements to the extinction coefficient for Ag$_2$ can be neglected under our experimental conditions.

Errors introduced by (1) and (4) would cause the value of ε_{Ag_2} to be too high, while errors in (3) would cause it to be too low. The extinction coefficient obtained here would be a lower limit if H$^+$ is lost to other reactions (unlikely), but any increase in the extinction coefficient would give a rate constant for the formation of Ag$_2$ that is higher than diffusion controlled (and thus not possible), which supports assumption (3). Assumption (2) is impossible to test, given that we do not have a "standard" solution of Ag$_2$. We believe that the errors are small and not enough to change the key conclusion that the reaction Ag^0 + Ag^0 → Ag$_2$ is diffusion controlled. The long times for the formation of Ag$_2$ in the LFP traces are due to the low initial concentration of Ag^0 (≤ 1 μM) generated in the reduction of Ag$^+$ after the laser pulse.

Scheme 4 depicts the two possible mechanisms by which Ag$_2$ clusters can form from reduced Ag^0. Reaction 8 in Scheme 4 would require that ketyl radicals persist in solution long enough for Ag$^+$ to react with Ag^0, hypothetically leading to Ag$_2^+$, and still be present at significantly high concentrations to react with Ag$_2^+$ to form Ag$_2$. This is very unlikely since the termination reactions are diffusion controlled and since the formation of Ag$_2$ fits to a second-order growth equation with a correlation of $R = 0.9945$, which is not necessarily expected for reaction 8. Therefore, reaction 5 in Scheme 4 better represents the mechanism.

Scheme 4. Possible Ag$_2$ Formation Reactions
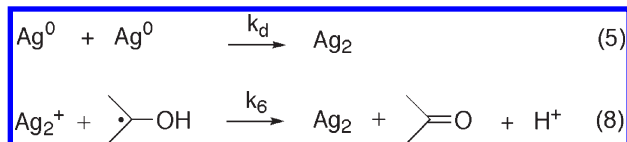
In an attempt to determine k_{et} in reaction 4 (Scheme 1), α-phenylbenzoin in toluene was used to determine the rate at which AgCF$_3$COO quenches ketyl radicals. It was found that the quenching of the ketyl radical by Ag$^+$ was barely competitive with other radical decay processes. In radical polymerization processes where the termination reactions are much faster than the polymerization, the rate of polymerization is known to follow a square root dependence on the light intensity.[9] This is reflected here as well in that reactions 2 and 3 approach diffusion control, and the competing reaction is not the formation of Ag$_2$ (reaction 5), which is fast, but rather the quenching of ketyl radicals by Ag$^+$ (reaction 4), which is relatively slow in toluene. Therefore, the square root dependence on the laser power shown in Figure 2 can be explained if $k_{et} \ll k_1 + k_2$.

The low quenching rate of α-phenylbenzoin with AgCF$_3$COO and the square root of the laser power dependence on the plateau of the ΔOD imply that reaction 4 (Scheme 1) is slower than reactions 2 and 3 in toluene, and much slower than quenching of ketyl radicals in aqueous solutions. Ketyl radicals are expected to react with Ag$^+$ in aqueous systems at a diffusion-controlled rate, just as Au^{3+} does.[17,18] The results here, on the other hand, suggest that ketyl radicals react with Ag$^+$ more slowly in nonpolar solvents. This may be related to the production of H$^+$ in reaction 4 that is easily stabilized in water, but not in nonpolar solvents like toluene. One of the roles of the amine in this work is to serve as a proton "sink" by acting as a base, as shown in Scheme 2. This does not require reaction 4 to be

reversible, but rather the presence of a kinetic barrier to H^+ release in nonpolar solvents.

Amines are also known to be NP stabilizing agents, as well as affecting the reduction potential of Ag^+/Ag^0; however, their role can be quite complex.[19] Equimolar amine is necessary for the long-term stability of fluorescent AgNP solutions,[5] but it is not essential to form an unstable Ag_2 signal at 450 nm in the LFP experiments (Supporting Information). While the overall yield of Ag_2 in an LFP experiment is strongly dependent on the concentration of CHA used, the rate of formation of Ag_2 is unaffected by the amine, as expected, since the observed kinetics are dominated by the major process (reactions 2 and 3). Thus, it would appear that proton capture by a base plays a key role as an enabling factor for reaction 4 to occur efficiently and irreversibly.

In the 1970s and 80s, several studies by Henglein examined the mechanism of formation of small Ag clusters by LFP of aqueous solutions of Ag^+.[20,21] These studies account for the short-term stability of small silver clusters by charge stabilization of Ag_n^+ clusters with $n \geq 2$. These small clusters had absorption maxima around 260 nm (dependent upon the size and charge of the clusters) that could be followed by transient spectroscopic techniques. The transient absorption of these charged clusters also decays on the time scale of milliseconds, and the decay corresponds well with the increase in absorption near 400 nm due to the formation of large clusters that support a surface plasmon.[21] On the other hand, the absorption of Ag_2 clusters that we observe has a maximum at 450 nm, approximately 200 nm red-shifted from that of the charged clusters observed by Henglein; their spectrum does not resemble that of positively charged silver clusters. Since most of our work is carried out in toluene, we expect that charged clusters would not be stabilized by the solvent, but the absorption at 450 nm also shows a long-term stability not seen for the charged clusters even in aqueous environments. Clearly the absorption at 450 nm cannot be due to charged metal clusters, but the increase in absorption shows no induction and plateaus in approximately 100 μs, which is 200 times faster than that observed for AgNP formation by Henglein as well. Figure 7 also exemplifies the differences in the absorbance observed by LFP for solutions that generate AgNP, showing that the intensity, rates, and absorption maxima for Ag_2 are all significantly different from those of AgNP by LFP; the latter is due to plasmon transitions. In flowing a solution to make nonfluorescent AgNP, the growth is presumably so slow (>milliseconds, reported by Henglein) that a change in absorbance at wavelengths from 400 to 500 nm could not be detected, but when the solution is not flowed, the change in ΔOD can be attributed to growth of existing AgNP. This growth happens by addition of Ag^0 to AgNP that were formed on previous laser pulses. Even in this case, the rate of growth is significantly slower than the rate of formation of Ag_2. Overall, the major conclusion to be taken from analysis of Figures 6 and 7 is that the absorption at 450 nm observed in AgFNP solutions cannot be attributed to the plasmon absorption for AgNP, which occurs at a different wavelength maximum and on a much slower time scale. This is consistent with the fact that the 450 nm signal could not be due to AgNP since the emission upon 450 nm excitation is quite intense, with a 2.6 ns lifetime, while the plasmon signal is extremely weak and has a femtosecond lifetime.

Overall, the second-order growth as $2Ag^0 \rightarrow Ag_2$, the intense emission of the silver clusters, and the position of the absorption maximum support the conclusions that the absorption at 450 nm is in fact due to Ag_2 clusters and that their rate of formation is diffusion controlled. The difference in reactivity in nonpolar solvents also suggests that the eventual formation of nanoparticles does not go through charged Ag_n^+ species, as was the result found by Henglein in aqueous systems, but rather via neutral Ag_n cluster intermediates.[20−22]

The particular selectivity for forming Ag_2 that is seen in the bleach and recovery experiment (Figure 5) and the two laser experiments (Figure 6) has some interesting possible implications. Due to the particular stability of Ag_2, it is difficult to imagine a route to the formation of AgNP (generated in AgFNP solutions as well) that involves Ag_3, because that would imply the addition of Ag^0 to an Ag_2 cluster, but Ag^0 seems to have a preference for dimerization. In fact, this implies that the early stages in the formation of AgNP in nonpolar solvents may in fact go through even-number atomic clusters as these Ag−Ag dimers aggregate.

■ CONCLUSION

In summary, we explored the formation of Ag_2 clusters through various LFP experiments where we determined that the rate constant for the formation of Ag_2 clusters is diffusion controlled. In a flow system (as used here) where no AgNP seeds are present, this must be the first step in the conception of the nascent AgNP. To the best of our knowledge, this is the first reported value for the rate constant for Ag^0−Ag^0 bond formation. This result is based on our estimation of $\varepsilon_{Ag_2} \approx 25\,400\ M^{-1}\ cm^{-1}$ for Ag_2. A mechanism for the formation of Ag_2 is also proposed, including a low rate constant for ketyl radical quenching by Ag(I) in toluene, something that most likely applies to other nonpolar media as well.

■ EXPERIMENTAL SECTION

To understand the formation and stability of Ag_2 in colloidal solutions leading to AgNP, the kinetics of the formation of Ag_2 were monitored using laser flash photolysis (LFP). Unless otherwise stated, typically toluene solutions for LFP experiments contained 10 mM $AgCF_3COO$ as Ag precursor, 5 mM Irgacure-2959 (I-2959) as a photochemical reducing agent, and 5 mM cyclohexylamine (CHA) as a NP stabilizing agent. I-2959 undergoes Norrish type I photocleavage, with a quantum yield of 0.29.[23] The ketyl radicals produced are strong reducing agents,[17] which reduce Ag^+ to Ag^0.[24] The absorption change at 450 nm due to Ag_2 formation was monitored over time.

The LFP setup is described in detail in the Supporting Information. Briefly, the LFP solutions were irradiated with a 355 nm, ~20 ns pulse width Nd:YAG laser to initiate the photocleavage of I-2959. The change in absorbance after each laser pulse is monitored with a customized Luzchem LFP system, and the transient data are recorded and averaged using Luzchem LFP software. It is important to note that the LFP solutions were normally flowed rapidly through a quartz cuvette to avoid bleaching of Ag_2 (evident when solutions are not flowed or are flowed slowly, see Figure 5) by subsequent laser pulses irradiating already reduced silver.

The AgNP that result after irradiation were deposited onto carbon-coated copper grids, and a JEOL JSM-7500F field emission scanning electron microscope equipped with a STEM detector was used to obtain low-resolution transmission SEM images of the AgNP (see Figure S3).

To obtain an extinction coefficient for Ag_2 (ε_{Ag_2}), bromothymol blue (BTB-H) was used as an indicator to quantify the remaining CHA in the basic form after some CHA was protonated by the H^+ (produced when Ag^+ quenches ketyl radicals to give Ag^0, as shown in Scheme 1, reaction 4). In this experiment, a typical LFP precursor solution (described above) is photolyzed with UVA irradiation in a Luzchem photoreactor, and the

3919

dx.doi.org/10.1021/ja108451v |*J. Am. Chem. Soc.* 2011, 133, 3913–3920

absorption spectrum of the resultant AgFNP is recorded using a Cary 100 UV–vis spectrometer. The photolyzed LFP solution is then added in small aliquots to a solution of BTB-H, and the absorption spectrum of the BTB-H solutions is recorded. The basic form of BTB has a strong absorption at 400 nm that was also monitored using a Cary 100 UV–vis spectrometer. The increase in absorbance at 400 nm in a BTB-H/BTB solution was monitored in two separate experiments where (1) a nonphotolyzed LFP solution and (2) a photolyzed AgFNP solution were added. The change in absorbance at 400 nm for BTB-H/BTB for the two parallel experiments was compared and used as a measure of the difference in CHA concentration and therefore a measure of the H^+, or in other words as a measure of Ag^0 that was reduced and eventually forms the Ag_2 clusters as described by reaction 4 in Scheme 1. It is important to note that small aliquots of the toluene solutions were added to much larger volumes of aqueous indicator solutions, in which case the CHA/CHA-H^+ were soluble and detected in the aqueous phase containing the indicator.

Nonfluorescent silver nanoparticles (AgNP) were also prepared using LFP, and the formation of particles that support a surface plasmon absorption was followed spectroscopically in order to rule out the possibility that the signal at 450 nm was a plasmon absorption of AgNP. For nonfluorescent AgNP, it has become common practice in our group to use varying concentrations of $AgNO_3$, I-2959, and trisodium citrate ([trisodium citrate] $\geq$ $AgNO_3$), as was the case here.[14] These aqueous solutions were purged with nitrogen and photolyzed in $7 \times 7\ mm^2$ cuvettes with the same LFP setup described above, but with a 266 nm laser in order to generate high concentrations of ketyl radicals that subsequently reduce Ag^+ to Ag^0.

■ ASSOCIATED CONTENT

Ⓢ Supporting Information. Detailed description of the LFP experimental setup; calculations and table of values used in determining the extinction coefficient for Ag_2; and data pertaining to the effect of the CHA concentration on the observed transient optical density for Ag_2. This material is available free of charge via the Internet at http://pubs.acs.org.

■ AUTHOR INFORMATION

Corresponding Author
tito@photo.chem.uottawa.ca

■ ACKNOWLEDGMENT

■ REFERENCES

(1) Zheng, J.; Nicovich, P. R.; Dickson, R. M. *Annu. Rev. Phys. Chem.* **2007**, *58*, 409–431.

(2) Xu, H.; Suslick, K. S. *ACS Nano* **2010**, *10*, 3209–3214.

(3) Yu, J.; Patel, S. A.; Dickson, R. M. *Angew. Chem., Int. Ed.* **2007**, *46*, 2028–2030.

(4) Guo, W.; Yuan, J.; Wang, E. *Chem. Commun.* **2009**, 3395–3397. Lee, T. H.; Gonzalez, J. I.; Zheng, J.; Dickson, R. M. *Acc. Chem. Res.* **2005**, *38*, 534–541.

(5) Maretti, L.; Billone, P. S.; Liu, Y.; Scaiano, J. C. *J. Am. Chem. Soc.* **2009**, *131*, 13972–13980.

(6) Watanabe, K.; Menzel, D.; Nilius, N.; Freund, H. J. *Chem. Rev.* **2006**, *106*, 4301–4320.

(7) Díez, I.; Pusa, M.; Kulmala, S.; Jiang, H.; Walther, A.; Goldmann, A. S.; Müller, A. H.; Ikkala, O.; Ras, R. H. *Angew. Chem., Int. Ed.* **2009**, *48*, 2122–2125. Guo, W.; Yuan, J.; Dong, Q.; Wang, E. *J. Am. Chem. Soc.* **2009**, *132*, 932–934. Jia, J.; Wang, Q. *J. Am. Chem. Soc.* **2009**, *131*, 16634–16635. Koenig, L.; Rabin, I.; Schulze, W.; Ertl, G. *Science* **1996**, *274*, 5291. Peyser, L. A.; Vinson, A. E.; Bartko, A. P.; Dickson, R. M. *Science* **2001**, *291*, 103–106. Rabin, I.; Schulze, W.; Ertl, G. *J. Chem. Phys.* **1998**, *108*, 5137–5141. Rabin, I.; Schulze, W.; Ertl, G.; Felix, C.; Sieber, C.; Sieber, C.; Buttet, J. *Chem. Phys. Lett.* **2000**, *320*, 59–64. Shen, Z.; Duan, H.; Frey, H. *Adv. Mater.* **2007**, *19*, 349–352. Vosch, T.; Antoku, Y.; Hsiang, J.; Richards, C. I.; Gonzalez, J. I.; Dickson, R. M. *Proc. Natl. Acad. Sci. U.S.A.* **2007**, *104*, 12616–12621. Zheng, J.; Dickson, R. M. *J. Am. Chem. Soc.* **2002**, *124*, 13982–139833.

(8) Takimoto, B.; Nabika, H.; Murakoshi, K. *J. Phys. Chem. C* **2009**, *113*, 11751–11755.

(9) Kochi, J. K. *Free Radicals*; Wiley: New York, 1973.

(10) Filipescu, N.; Minn, F. L. *J. Am. Chem. Soc.* **1968**, *90*, 1544–1547.

(11) Scaiano, J.; Abuin, E. B. *Chem. Phys. Lett.* **1981**, *81*, 209–213. Scaiano, J.; Abuin, E. B.; Stewart, L. C. *J. Am. Chem. Soc.* **1982**, *104*, 5673–5679.

(12) Green, F. J. *The Sigma-Aldrich Handbook of Stains, Dyes and Indicators*, 2nd ed.; Aldrich Chemical Co. Inc.: Madison, WI, 1990. Sinisterra, J. V.; Blanco, F. G.; Iglesias, M.; Marinas, J. M. *React. Kinet. Catal. Lett.* **1984**, *25*, 277–282.

(13) Ramamurthy, V.; J. Turro, N.; Scaiano, J. C. *Modern Molecular Photochemistry of Organic Molecules*; University Science Publishers: New York, 2010.

(14) Stamplecoskie, K. G.; Scaiano, J. C. *J. Am. Chem. Soc.* **2010**, *132*, 1825–1827.

(15) Lipscher, J.; Fischer, H. *J. Phys. Chem.* **1984**, *88*, 2555–2559.

(16) Vosch, T.; Antoku, Y.; Hsiang, J. C.; Richards, C. I.; Gonzalez, J. I.; Dickson, R. M. *Proc. Natl. Acad. Sci. U.S.A.* **2007**, *104*, 12616–12621.

(17) Marin, M. L.; McGilvray, K. L.; Scaiano, J. C. *J. Am. Chem. Soc.* **2008**, *130*, 16572–16584. McGilvray, K. L.; Decan, M. R.; Wang, D.; Scaiano, J. C. *J. Am. Chem. Soc.* **2006**, *128*, 15980–15981.

(18) Scaiano, J. C.; Billone, P.; Gonzalez, C. M.; Maretti, L.; Marin, M. L.; McGilvray, K. L.; Yuan, N. *Pure Appl. Chem.* **2009**, *81*, 635–647.

(19) Frattini, A.; Pellegri, N.; Nicastro, D.; Sanctis, O. *Mater. Chem. Phys.* **2005**, *94*, 148–152. Texier, I.; Rmita, S.; Archirel, P.; Mostafavi, M. *J. Phys. Chem.* **1996**, *100*, 12472–12476.

(20) Henglein, A. *Chem. Rev.* **1989**, *89*, 1861–1873.

(21) Henglein, A.; Tausch-Treml, R. *J. Colloid Interface Sci.* **1980**, *80*, 84–93.

(22) Mpourmpakis, G.; Vlachos, D. G. *Langmuir* **2008**, *24*, 7465–7743.

(23) Jockusch, S.; Landis, M. S.; Freiermuth, B.; Turro, N. J. *Macromolecules* **2001**, *34*, 1619–1626.

(24) Scaiano, J. C.; Aliaga, C.; Maguire, S.; Wang, D. *J. Phys. Chem. B* **2006**, *110*, 12856–12859.

3920

dx.doi.org/10.1021/ja108451v |*J. Am. Chem. Soc.* 2011, 133, 3913–3920